

Energy-Efficiency and Spectral-Efficiency Trade-off in Distributed Massive-MIMO Networks

Mohd Saif Ali Khan*, Samar Agnihotri* and Karthik R.M.†

*School of Computing & EE, Indian Institute of Technology Mandi, HP, India

†Ericsson India Global Services Pvt. Ltd., Chennai, TN, India

Email: d21013@students.iitmandi.ac.in, samar@iitmandi.ac.in,
karthik.r.m@ericsson.com

Abstract

This paper investigates the inherent trade-off between energy efficiency (EE) and spectral efficiency (SE) in distributed massive-MIMO (D-mMIMO) systems. Optimizing the EE and SE together is crucial as increasing spectral efficiency often leads to higher energy consumption. Joint power allocation and AP-UE association are pivotal in this trade-off analysis because they directly influence both EE and SE. We address the gap in existing literature where the EE-SE trade-off has been analyzed but not optimized in the context of D-mMIMO systems. The focus of this study is to maximize the EE with constraints on uplink sum SE through judicious power allocation and AP-UE association, essential for enhancing network throughput. Numerical simulations are performed to validate the proposed model, exploring the impacts of AP-UE association and power allocation on the EE-SE trade-off in uplink D-mMIMO scenarios.

Index Terms

Distributed Massive MIMO, AP-UE Association, Power Control, Energy & Spectral Efficiency Trade-off

I. INTRODUCTION

In the era of 5G and beyond, the fast expansion of connected devices and exponential rise in data traffic have made spectral efficiency (SE) and energy efficiency (EE) key network design factors. Enhanced SE is desirable to meet the growing demand for higher data rates and better

quality of service, but it often comes at the cost of significantly increased energy consumption due to higher power demands on infrastructure and devices. As we increasingly move toward green communication, optimizing the EE and SE becomes a critical challenge in 5G networks, where technologies such as massive MIMO and dense deployment of access points aim to boost SE, but may increase energy consumption to unsustainable levels, both environmentally and economically. Therefore, striking a balance between SE and EE is not only desirable technically, but is also a critical step towards sustainable communication systems.

Distributed massive-MIMO (D-mMIMO) combines the advantages of massive-MIMO and the cell-free architecture to improve performance of the network [1]. The D-mMIMO systems provide uniform service quality over a coverage area by distributing antennas across the region, enhancing both EE and SE compared to conventional cellular networks [2].

In general, there is an inherent trade-off between the EE and SE, increasing the SE may lead to a decrease in the EE, and vice versa. This trade-off can also be observed in D-mMIMO systems. In [3], the authors have analyzed the EE-SE trade-off for downlink scenarios, but the EE and SE are not optimized. In D-mMIMO systems, two of the primary factors that influence both EE and SE are power allocation and AP-UE association, where each user is dynamically associated with a subset of APs that collaboratively serve the user [2]. Thus, the joint power allocation and AP-UE association is important to enhance the energy and spectral efficiencies of D-mMIMO networks and to analyze their trade-off.

Much work has been done for power allocation and AP-UE association to enhance either SE or EE of the D-mMIMO systems [2], [4]–[11]. But none of the existing work, to the best of our knowledge, deals with the EE-SE trade-off while performing AP-UE association and power allocation for the D-mMIMO. Our work attempts to address this gap.

We formulate an optimization problem for EE maximization with a constraint on the quality-of-service (QoS) requirement of the sum SE with respect to power allocation and AP-UE association. The goal is to establish a trade-off between EE and SE while finding the power allocation across APs and the association between APs and UEs that maximize network performance under these constraints.

Organization: Section II presents the system model. Section III details the problem formulation. Section IV introduces our proposed solution and establishes its convergence. In Section V, using the proposed solution approach, we numerically evaluate the trade-off between the EE and SE with respect to various system parameters. Finally, Section VI concludes our work and

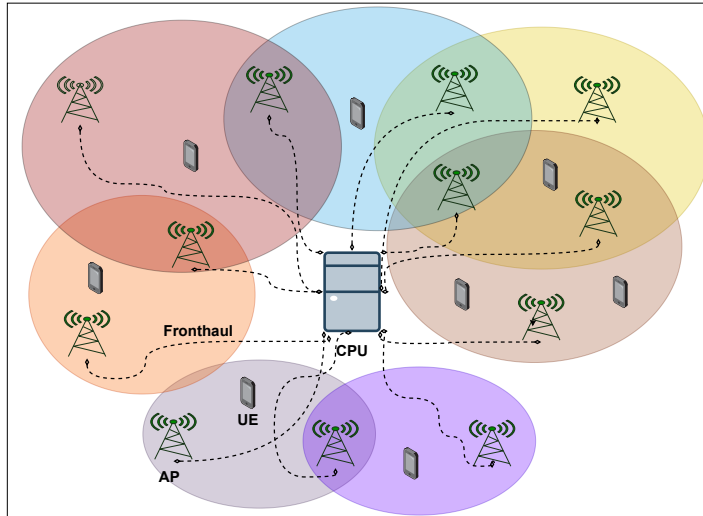


Fig. 1. A typical network model. Here each colored oval identifies the UE(s) and the APs that serve it(them).

provides some directions for future work.

II. SYSTEM MODEL

We consider a scenario where T single antenna UEs and M multi-antenna APs operate within a defined coverage area. Each AP is equipped with A antennas, and the relationship $T \ll MA$ indicates a high antenna-to-user ratio, facilitating substantial spatial multiplexing gains. The APs and the UEs are uniformly distributed across the coverage area, ensuring that every UE is within the service range of multiple APs. All APs can serve all UEs simultaneously using the same time and frequency resources. Connectivity between the APs and the central processing unit (CPU) is ensured via a front-haul link, which is critical for coordinating signal processing tasks and distributing user data and control information efficiently across the network. To ensure network scalability, a user-centric approach has been adopted, where each UE is served by a subset of APs, as depicted in Fig. 1.

This setup uses Time-Division Duplexing (TDD) mode for communication. Channel estimation is conducted during the uplink phase where the UEs transmit orthogonal pilot signals, and the APs estimate the uplink channel vectors. The system employs a block fading model, characterized by a coherence block of length L_c . Within each block, a portion defined by L_p is dedicated to pilot transmission for channel estimation. The small-scale fading component, denoted by $\mathbf{h}_{mt} \in \mathbb{C}^{A \times 1}$, follows a Rayleigh distribution. Each component of \mathbf{h}_{mt} is assumed to be an independent and identically distributed (i.i.d.) complex Gaussian random variable with zero mean

and unit variance. Large-scale fading coefficient (LSFC), denoted by β_{mt} , accounts for path-loss and shadowing effects. The overall channel vector $\mathbf{g}_{mt} \in \mathbb{C}^{A \times 1}$ is given by $\mathbf{g}_{mt} = \beta_{mt}^{1/2} \mathbf{h}_{mt}$.

A. Uplink Pilot Training

We assume that during uplink channel estimation, each UE t transmits the pilot sequence $\sqrt{L_p} \Psi_t \in \mathbb{C}^{L_p \times 1}$, such that $\|\Psi_t\|^2 = 1$. The received signal $\mathbf{y}_m^{pilot} \in \mathbb{C}^{A \times L_p}$ is given by :

$$\mathbf{y}_m^{pilot} = \sum_{t=1}^T \sqrt{L_p p_p} \mathbf{g}_{mt} \Psi_t^H + \mathbf{N}_m,$$

where $\mathbf{N}_m \in \mathbb{C}^{A \times L_p}$ is the complex additive white Gaussian noise matrix with each element distributed normally with zero mean and unit variance. Also, p_p represents the normalized signal-to-noise power for pilot transmission. The mean square value of any component of MMSE-estimated channel vector \mathbf{g}_{mt} is given by [2]: $\gamma_{mt} = \frac{L_p p_p \beta_{mt}^2}{\sum_{t'=1}^T L_p p_p \beta_{mt'} |\Psi_t^H \Psi_{t'}|^2 + 1}$.

B. Uplink Data Transmission

The uplink signal received at the m^{th} AP is given by:

$$\mathbf{y}_m^u = \sqrt{p_u} \sum_{t \in \mathcal{T}} \mathbf{g}_{mt} \sqrt{\eta_t^u} x_t + \mathbf{n}_m,$$

where x_t is the uplink payload signal transmitted from the UE t , such that $\mathbb{E}\{|x_t|^2\} = 1$. The uplink normalized signal-to-noise power and power control coefficient of the UE t are denoted by p_u and η^u , respectively. Also, \mathbf{n}_m is the complex additive white Gaussian noise matrix with each element distributed normally with zero mean and unit variance. The large scale fading decoding (LSFD) of the UE t for all APs is performed at CPU after local data estimation using the combining vector, \mathbf{v}_{mt} for APs m , as: $\hat{y}_t = \sum_{m=1}^M d_{mt} \mathbf{v}_{mt}^H \mathbf{y}_m^u$, where d_{mt} is the AP-UE association binary variable of the UE t for AP m such that when AP m serves the UE t , then $d_{mt} = 1$, else $d_{mt} = 0$.

C. Spectral Efficiency and Energy Efficiency

The uplink spectral efficiency of the UE t and of the overall system are given by:

$$\begin{aligned} \text{SE}_t^u &= w \log_2(1 + \Gamma_t), \\ \text{SE}^u|_{\Gamma_t} &= \sum_{t=1}^T \text{SE}_t^u, \end{aligned}$$

where $w = (1 - \frac{L_p}{L_c})$ and Γ_t is the effective uplink signal-to-interference-noise ratio (SINR) of the UE t .

The closed-form expression of effective SINR for any UE t the partial full-pilot zero-forcing (PFZF) combining [12] is given by $\Gamma_t = DS_t/I_t$, where

$$\begin{aligned} DS_t &= \eta_t^u p_u \left| \sum_{m \in \mathcal{Z}_t} d_{mt} \gamma_{mt} + A \sum_{m \in \mathcal{Q}_t} d_{mt} \gamma_{mt} \right|^2, \\ I_t &= \mathbf{A}_t^P + \mathbf{B}_t^P + \mathbf{C}_t^P, \\ \mathbf{A}_t^P &= \sum_{t'=1}^T \eta_{t'}^u p_u \left(\sum_{m \in \mathcal{Z}_t} \frac{d_{mt}^2 \gamma_{mt} (\beta_{mt'} - \gamma_{mt'})}{A - L_{S_m}} + A \sum_{m \in \mathcal{Q}_t} d_{mt}^2 \gamma_{mt} \beta_{mt'} \right) \\ \mathbf{B}_t^P &= \sum_{t' \in \mathcal{P}_t / \{t\}} \eta_{t'}^u p_u \left| \sum_{m \in \mathcal{Z}_t} \frac{d_{mt} \gamma_{mt} \sqrt{\eta_{t'} \beta_{mt'}}}{\sqrt{\eta_t} \beta_{mt}} + A \sum_{m \in \mathcal{Q}_t} \frac{d_{mt} \gamma_{mt} \sqrt{\eta_{t'} \beta_{mt'}}}{\sqrt{\eta_t} \beta_{mt}} \right|^2 \\ \mathbf{C}_t^P &= \sum_{m \in \mathcal{Z}_t} d_{mt}^2 \frac{\gamma_{mt}}{A - L_{S_m}} + A \sum_{m \in \mathcal{Q}_t} d_{mt}^2 \gamma_{mt}. \end{aligned}$$

The total uplink energy efficiency of the network in bits per joule is defined as: $EE = \frac{B SE^u|_{\Gamma_t}}{P_T}$, where B is the total bandwidth and according to [13]:

$$\begin{aligned} P_T &= P_T^{\text{fix}} + P_T^c + P_{cpu}^{\text{deco}} B SE^u|_{\Gamma_t}, \\ P_T^c &= \sum_{t=1}^T \left(\frac{\eta_t^u p_n p_u}{\zeta} + \sum_{m=1}^M (d_{mt} P_{cpu}^{\text{lsfd}} + A d_{mt} P^{\text{proc}} + d_{mt} P^{\text{sig}}) \right), \\ P_T^{\text{fix}} &= T P_{ue}^c + M A P_{ap}^c + M P_{fh}^{\text{fix}} + P_{cpu}^{\text{fix}}, \end{aligned}$$

and P_{ue}^c , P_{ap}^c , P^{proc} , P_{fh}^{fix} , P^{sig} , P_{cpu}^{fix} , P_{cpu}^{lsfd} and P_{cpu}^{deco} are defined as circuit power of UE, circuit power of the AP, power required for signal processing at the AP, fronthaul linked fix power, signaling power for a fronthaul link, CPU fixed power consumption, power required for LSFD and signal decoding power at the CPU, respectively. Also, $0 < \zeta \leq 1$ is the power amplifier efficiency and p_n is the noise power.

III. PROBLEM FORMULATION

We introduce an optimization problem formulation for maximizing EE that involves allocating power to all UEs and determining AP-UE allocations, subject to the constraint of achieving a

minimum total SE as follows.

$$\max_{\boldsymbol{\eta}^u, \mathbf{D}} \frac{B \text{SE}^u |_{\Gamma_t}}{P_T^{\text{fix}} + P_T^c + P_{cpu}^{\text{deco}} B \text{SE}^u |_{\Gamma_t}}, \quad (1a)$$

$$\text{subject to: } d_{mt} \in \{0, 1\}, \forall m \in \mathcal{M}, t \in \mathcal{T}, \quad (1b)$$

$$0 \leq \eta_t^u \leq 1, \forall t \in \mathcal{T}, \quad (1c)$$

$$\text{SE}^u |_{\Gamma_t} \geq \text{SE}^{\text{QoS}}, \forall t \in \mathcal{T}, \quad (1d)$$

$$\sum_{m=1}^M d_{mt} \geq 1, \forall t \in \mathcal{T}, \quad (1e)$$

where $\boldsymbol{\eta}^u = \{\eta_t^u\}_{t \in \mathcal{T}}$ and \mathbf{D} is the AP-UE association matrix with each element as d_{mt} . \mathbf{D}_t represents the column vector of matrix \mathbf{D} with respect to the UE t . The regularization coefficient $\alpha \geq 0$ is the trade-off factor between the front-haul load and the SE. SE^{QoS} represents the minimum QoS requirement. Constraint (1b) represents the binary variable indicating the association between the UEs and APs. Constraint (1c) represents the uplink power control coefficient. Constraint (1d) is for the minimum QoS requirement and constraint (1e) specifies that at least one AP must be connected to the UE.

This problem is an instance of mixed-integer non-linear programming (MINLP) problems which are, generally, NP-hard. We employ the Successive Convex Approximation (SCA) technique [14] to find an approximate but lower complexity solution for it, as described next.

IV. THE SCA BASED ENERGY EFFICIENCY MAXIMIZATION

We provide an approach to find a feasible solution to Problem (1). The proposed approach employs various relaxations and approximations steps, as outlined and discussed below:

Step 1: In the objective function (1a), the numerator and denominator both contain the sum SE term. So, we reformulate the optimization problem to reduce its solution complexity by maximizing a new objective function $\frac{B \text{SE}^u |_{\Gamma_t}}{P_T^{\text{fix}} + P_T^c}$. It should be noted that maximizing the new objective function is same as maximizing the original objective function in (1a), thus preserving the optimality of the solution.

Step 2: We relax the binary variable d_{mt} to a continuous one to convert the given MINLP problem to a non-linear programming (NLP) problem, to write constraint (1b) as:

$$0 \leq d_{mt} \leq 1, \forall m \in \mathcal{M}, t \in \mathcal{T}. \quad (2)$$

Remark : In the new objective function, the power consumption term behaves as the penalty for the AP-UE association matrix, forcing the d_{mt} to take values either close to one or zero. Thus, maintaining the feasibility of our original constraint (1b).

Step 3: Given that Γ_t is non-linear, we introduce an auxiliary variable Γ_t^* as the lower bound on Γ_t . This substitution removes the non-linearity from the logarithmic term by replacing Γ_t with Γ_t^* in both the new objective function and constraint (1d). Consequently, a new constraint is introduced in the reformulated problem to ensure the feasibility of the new variable Γ_t^* . The additional constraint is given as:

$$\Gamma_t^* \leq \Gamma_t, \quad t \in \mathcal{T}. \quad (3)$$

However, this constraint is non-convex due to the fractional non-convex term, Γ_t . Thus, to make it tractable, we use the quadratic transformation [15], and replace constraint (3) by:

$$\Gamma_t^* \leq 2z_t\sqrt{DS_t} - z_t^2I_t. \quad (4)$$

The feasibility of constraint (4) lies in the fact that $\Gamma_t \geq 2z_t\sqrt{DS_t} - z_t^2I_t$. Thus, satisfying constraint (4) implies the satisfaction of constraint (3). Also, constraint (4) is marginally concave in z_t and the optimal value of z_t is given by $z_t^* = \sqrt{DS_t}/I_t$. Therefore, Problem (1) after incorporating the new auxiliary variable Γ_t^* and constraint (4) becomes:

$$\max_{\boldsymbol{\eta}^u, \mathbf{D}, \mathbf{z}, \boldsymbol{\Gamma}^*} \frac{B \text{SE}^u |_{\boldsymbol{\Gamma}^*}}{P_T^{\text{fix}} + P_T^c}, \quad (5a)$$

$$\text{subject to: } \text{SE}^u |_{\boldsymbol{\Gamma}^*} \geq \text{SE}^{\text{QoS}}, \forall t \in \mathcal{T}, \quad (5b)$$

$$(1c), (1e), (2), (4). \quad (5c)$$

where $\mathbf{z} = \{z_t\}_{t \in \mathcal{T}}$ and $\boldsymbol{\Gamma}^* = \{\Gamma_t^*\}_{t \in \mathcal{T}}$. In order to solve Problem (5), constraint (4) attempts to achieve equality. The value of z_t in (4) needs to be updated after each iteration by its optimal value, z_t^* . After substitution of z_t value in (4), constraint (4) becomes equivalent to constraint (3). As the iterations proceeds in our proposed iterative solution, Γ_t^* become equal to Γ_t . This implies that solving Problem (5) is equivalent to solving Problem (1).

Step 4: As objective function (5a) is in a fractional form, so to have a more tractable solution, we introduce two new variable u and v for the numerator and denominator, respectively. Thus,

the new problem becomes:

$$\max_{\boldsymbol{\eta}^u, \mathbf{D}, \mathbf{z}, \Gamma^*, u, v} \frac{u}{v}, \quad (6a)$$

$$\text{subject to: } \text{SE}^u|_{\Gamma_t^*} \geq \text{SE}^{\text{QoS}}, \forall t \in \mathcal{T}, \quad (6b)$$

$$B \text{SE}^u|_{\Gamma_t^*} \geq u, \quad (6c)$$

$$P_T^{\text{fix}} + \bar{P}_T \leq v, \quad (6d)$$

$$(1c), (1e), (2), (4). \quad (6e)$$

Solving Problem (6) is equivalent to solving (5) as constraints (6c) and (6d) must attain equality as iterations proceed. Still, we need to handle the fractional objective function (6a). The objective function (5a), which is a ratio of linear terms can be approximated using the quadratic transformation [15] as:

$$\frac{u}{v} \geq 2b\sqrt{u} - b^2v, \quad (7)$$

Since, $2b\sqrt{u} - b^2v$ is the lower bound to $\frac{u}{v}$, and thus maximizing $2b\sqrt{u} - b^2v$ also maximizes $\frac{u}{v}$. Therefore this transformation does not impact the feasibility of objective function (6a). Also, $2b\sqrt{u} - b^2v$ is marginally concave in b , and thus the optimal value of b is given by:

$$b^* = \frac{\sqrt{B \text{SE}^u|_{\Gamma_t^*}}}{P_T^{\text{fix}} + P_T^c}. \quad (8)$$

The new formulation can be rewritten as:

$$\max_{\boldsymbol{\eta}^u, \mathbf{D}, u, v, b, \mathbf{z}, \Gamma^*} 2b\sqrt{u} - b^2v, \quad (9a)$$

$$\text{subject to: } (1c), (1e), (2), (4), (5b), (6c), (6d). \quad (9b)$$

The value of b in objective function (9a) is updated using equation (8) after each iteration. As the iterations proceed, the objective function (9a) tries to achieve the same values as the objective function (6a). This establishes that solving Problem (9) is equivalent to solving Problem (6).

Step 5: After fixing the parameters b and \mathbf{z} , the only non-convex term in the above formulation (9) is constraint (4) due to the coupling of $\boldsymbol{\eta}^u$ and \mathbf{D} , which is further handled in the same way as in [11], to ensure the overall problem becomes convex and tractable. It should be noted that, the right side of constraint (4) is bi-concave in $\boldsymbol{\eta}^u$ and \mathbf{D} . Thus, Problem (9) can be solved by

an alternate optimization technique. First, we fix \mathbf{D} , b and \mathbf{z} , and solve:

$$f_1 = \max_{\boldsymbol{\eta}^u, u, v, \Gamma^*} 2b\sqrt{u} - b^2v, \quad (10a)$$

$$\text{subject to: } (1c), (4), (5b), (6c), (6d). \quad (10b)$$

After solving Problem (10), we calculate the b and \mathbf{z} . Then, we fix the $\boldsymbol{\eta}^u$, b and \mathbf{z} , then solve:

$$f_2 = \max_{\mathbf{D}, u, v, \Gamma^*} 2b\sqrt{u} - b^2v, \quad (11a)$$

$$\text{subject to: } (1e), (2), (4), (5b), (6c), (6d). \quad (11b)$$

Step 6: After solving Problem (11), we again calculate b and \mathbf{z} and then solve Problem (10).

The exact iterative steps are captured Algorithm 1.

Algorithm 1 The Proposed Algorithm

- 1: **Feasible Initialization:** $\boldsymbol{\eta}^{u(0)}$, $\mathbf{D}^{(0)}$ and $i = 0$, $\forall t \in \mathcal{T}$, $\epsilon = 5e^{-3}$.
 - 2: **repeat**
 - 3: $i = i + 1$.
 - 4: **for all** t **do**
 - 5: Calculate z_t .
 - 6: **end for**
 - 7: Calculate b using (8).
 - 8: Solve optimization problem in (10) for $\boldsymbol{\eta}^{u(i)}$.
 - 9: **for all** t **do**
 - 10: Re-calculate z_t .
 - 11: **end for**
 - 12: Re-calculate b using (8).
 - 13: Solve optimization problem in (11) for $\mathbf{D}^{(i)}$.
 - 14: Update $\boldsymbol{\eta}^{u(i+1)} = \boldsymbol{\eta}^{u(i)}$ and $\mathbf{D}^{(i+1)} = \mathbf{D}^{(i)}$.
 - 15: **until** $\left| \frac{f_2^{(i+1)} - f_2^{(i)}}{f_2^{(i)}} \right| \leq \epsilon$.
-

Convergence Analysis : To demonstrate the non-decreasing nature of the optimization function $f(\boldsymbol{\eta}^u, \mathbf{D}) = 2b\sqrt{u} - b^2v$, assume that $\boldsymbol{\eta}^{u^*}$ represents the optimal value of f , when \mathbf{D} is fixed. Given this, the inequality $f(\boldsymbol{\eta}^{u^*}, \mathbf{D}^{(i)}) \geq f(\boldsymbol{\eta}^{u(i)}, \mathbf{D}^{(i)})$ always holds due to the concavity of the function f with respect to $\boldsymbol{\eta}^u$. When optimizing \mathbf{D} to \mathbf{D}^* , with $\boldsymbol{\eta}^u$ fixed at $\boldsymbol{\eta}^{u^*}$, the inequality $f(\boldsymbol{\eta}^{u^*}, \mathbf{D}^*) \geq f(\boldsymbol{\eta}^{u^*}, \mathbf{D}^{(i)})$ always holds as f is concave with respect to \mathbf{D} . Therefore, combining these observations, we see that $f(\boldsymbol{\eta}^{u(i+1)}, \mathbf{D}^{(i+1)}) \geq f(\boldsymbol{\eta}^{u(i)}, \mathbf{D}^{(i)})$, indicating f is non-decreasing at each iteration. This non-decreasing trend makes the optimization function monotonically

increasing in each iteration and also the optimization function is bounded from above, ensuring the convergence of the optimization algorithm, as the function does not increase indefinitely but plateaus at the maximum value.

V. NUMERICAL SIMULATIONS

We conduct numerical simulations over a geographic area of 1×1 square kilometer with APs and UEs distributed randomly. To emulate an infinitely large network, we employ a wrap-around topology [8]. The LSFCs follow a three-slope path loss model, with shadow fading modeled by an 8 dB standard deviation. In simulations, we fix $T = 30$, $M = 40$, $A = 8$, $L_c = 200$, and $L_p = 5$. Unless mentioned otherwise, other parameters remain consistent with those in [2]. We average the numerical results across 100 simulation runs.

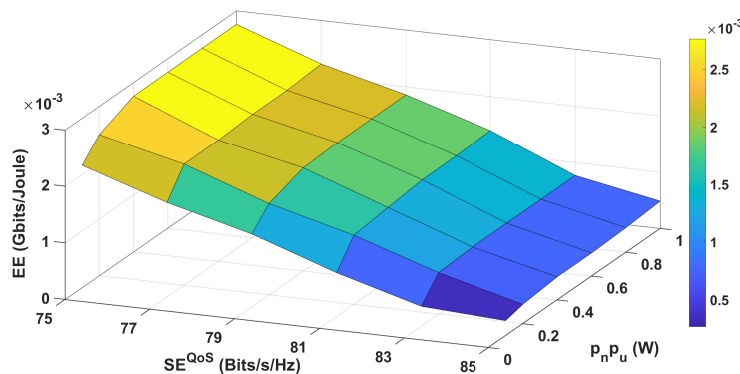


Fig. 2. The EE versus the sum SE threshold versus the maximum power.

Fig. 2 represents the 3-D plot among the EE, the sum SE threshold, and the maximum uplink power ($p_n p_u$) that UEs can attain. In this plot, the sum SE threshold varies from 75 to 85 Bits/s/Hz, and the maximum uplink UE power is varied from 0.1 to 1 W. For the maximum power level of 0.1 W, EE decreases from 2.16×10^{-3} to 2.64×10^{-4} Gbits/Joule as the SE^{QoS} increases from 75 to 85 Bits/s/Hz. A similar trend is observed at the power level of 0.2 W, the EE reduces from 2.5×10^{-3} to 3.42×10^{-4} Gbits/Joule for the same increase in the SE^{QoS} . This decreasing pattern persists across higher power levels from 0.4 to 1 W, consistently showing a reduction in EE as SE^{QoS} increases. This decline is attributed to the necessity of either allocating more APs to UEs, increasing the power allocated to UEs, or both, to enhance the SE. Consequently, this increases the overall power consumption and diminishes the network's EE. We note an increase in the EE with rising maximum uplink power up to a certain point for the fixed sum SE threshold. Notably, the EE begins to saturate beyond the power level of 0.4 W for lower SE^{QoS} . The optimization

algorithm, thereby, increases power consumption only when it contributes to the enhanced EE. For, the higher SE^{QoS} , however, the EE continues to increase with the rise in maximum power level, indicating that higher power levels contribute more significantly to achieving higher SE.

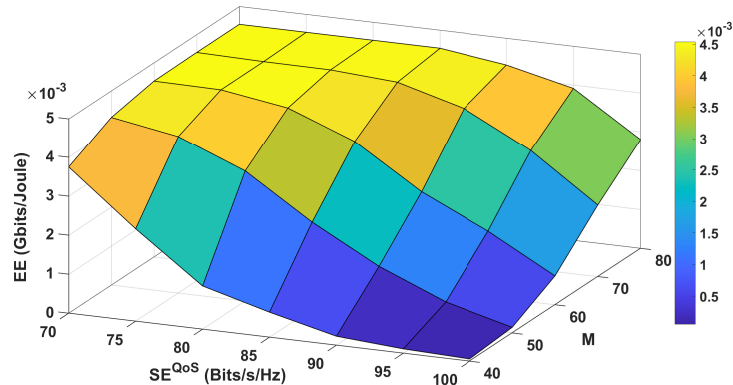


Fig. 3. The EE versus the sum SE threshold versus the number of APs for $p_n p_u = 0.1$.

Fig. 3 represents the 3-D plot among the EE, sum SE threshold, and number of APs (M). For $M = 40$, the EE decreases from 3.75×10^{-3} to 5.49×10^{-5} Gbits/Joule as the SE^{QoS} increases from 70 to 100 Bits/s/Hz. A similar trend is observed at $M = 80$, the EE declines from 4.53×10^{-3} to 2.8×10^{-3} Gbits/Joule for the same increase in SE^{QoS} . This decreasing pattern persists as the number of APs increases from 40 to 80, consistently showing a reduction in the EE as SE^{QoS} rises. This consistent decrease across AP configurations indicates that higher spectral efficiency necessitates more power per unit of data transmitted, thereby reducing the EE. For the fixed SE^{QoS} , we observe an increase in the EE with the increase in the number of APs. This indicates that the rate of increase in the SE is more than the rate of increase in circuit power due to the increase in the number of APs. However, this increase is modest at lower SE^{QoS} values such as 70 and 75 Bits/s/Hz. For the lower values of M , the optimization algorithm is easily able to achieve these lower SE^{QoS} values without allocating more APs to UEs, thus not increasing the power consumption. For higher values of M , due to increase in the circuit power, the total power consumption increases. However, with more APs, the likelihood of having APs closer to UEs increases, resulting in stronger channel condition. This proximity enhances both the SE and the EE by offsetting the impact of increased circuit power. For the higher SE^{QoS} values, when the number of APs are low, in order to maintain the high sum SE, the optimization algorithm allocates more APs to UEs, thus significantly reducing the EE due to increase in power consumption. However, when the number of APs is larger for these higher

SE^{QoS} values, the optimizing algorithm allocates fewer APs per UEs, hence reducing the power consumption and thus enhancing the EE.

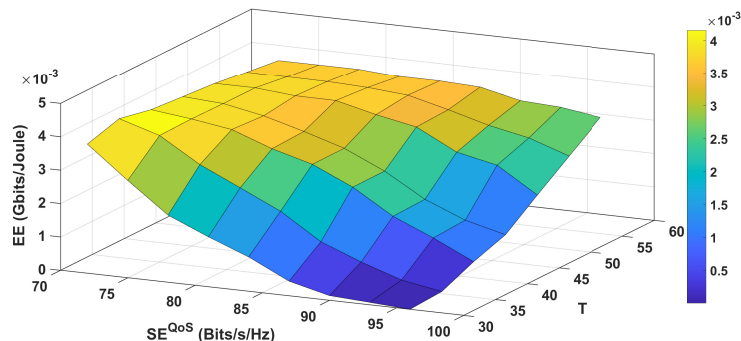


Fig. 4. The EE versus the sum SE threshold versus the number of UEs for $p_n p_u = 0.1$.

Fig. 4 shows the 3-D plot among the EE, the sum SE threshold, and the number of UEs (T). For a fixed T , an increase in the SE^{QoS} leads to a decline in EE. At lower SE^{QoS} values, the EE initially increases with T but eventually decreases when T becomes very high. This decline is attributed to the increased circuit power consumption required to accommodate more users at lower SE^{QoS} values. Conversely, at higher SE^{QoS} values, the EE consistently improves as a larger number of UEs facilitates achieving these higher SE^{QoS} values.

VI. CONCLUSION AND FUTURE WORK

This work has systematically explored the complex relationships among energy efficiency, spectral efficiency, and resource allocation parameters such as the number of APs and uplink power levels in distributed massive-MIMO (D-mMIMO) systems. A consistent trade-off between EE and SE is evident across different system configurations and parameters. As the SE demand increases, the EE generally decreases, indicating that higher data transmission rates necessitate greater power expenditure. This work also indicates the role of power allocation and the AP-UE association to achieve desired SE, while maintaining the satisfactory EE. The insights from this study underscore the necessity for sophisticated resource allocation strategies that prioritize both EE and SE, which is especially crucial in the era of 5G and 5G Advanced technologies. These technologies, generally, enhance SE but increase power consumption as well, making the study of this trade-off essential to maintain the environmental and the economic sustainability.

A compelling future direction involves drawing detailed comparisons of the EE-SE trade-offs across different network architectures, including small-cell networks, traditional mMIMO and

the D-mMIMO. Additionally, the influence of modulation and coding schemes, which is not considered in this study, presents another direction for exploration.

REFERENCES

- [1] M. S. A. Khan, S. Agnihotri, and R. Karthik, "Distributed Pilot Assignment for Distributed Massive-MIMO Networks," in *Proc. IEEE WCNC*, Dubai, UAE, April 2024.
- [2] H. Q. Ngo, A. Ashikhmin, H. Yang, E. G. Larsson, and T. L. Marzetta, "Cell-free massive MIMO versus small cells," *IEEE Trans. on Wireless Commun.*, vol. 16, no. 3, pp. 1834–1850, 2017.
- [3] Y. Huang, Y. Jiang, F.-C. Zheng, P. Zhu, D. Wang, and X. You, "Performance of spectral and energy efficiency in cell-free massive MIMO-aided URLLC system with short blocklength communications," *IEEE Trans. on Veh. Techno.*, vol. 73, no. 9, pp. 13,023–13,037, 2024.
- [4] H. Q. Ngo, L.-N. Tran, T. Q. Duong, M. Matthaiou, and E. G. Larsson, "On the total energy efficiency of cell-free massive MIMO," *IEEE Trans. on Green Commun. and Network.*, vol. 2, no. 1, pp. 25–39, 2017.
- [5] T. X. Vu, S. Chatzinotas, S. ShahbazPanahi, and B. Ottersten, "Joint power allocation and access point selection for cell-free massive MIMO," in *Proc. IEEE ICC*, Online, June 2020.
- [6] H. Q. Ngo, H. Tataria, M. Matthaiou, S. Jin, and E. G. Larsson, "On the performance of cell-free massive MIMO in Ricean fading," in *Proc. IEEE ACSSC*, Pacific Grove, CA, USA, Oct. 2018.
- [7] M. Guenach, A. A. Gorji, and A. Bourdoux, "Joint power control and access point scheduling in fronthaul-constrained uplink cell-free massive MIMO systems," *IEEE Trans. on Commun.*, vol. 69, no. 4, pp. 2709–2722, 2020.
- [8] E. Björnson and L. Sanguinetti, "Scalable cell-free massive MIMO systems," *IEEE Trans. on Commun.*, vol. 68, no. 7, pp. 4247–4261, 2020.
- [9] T. C. Mai, H. Q. Ngo, and L.-N. Tran, "Energy efficiency maximization in large-scale cell-free massive MIMO: A projected gradient approach," *IEEE Trans. on Wireless Commun.*, vol. 21, no. 8, pp. 6357–6371, 2022.
- [10] C. Hao, T. T. Vu, H. Q. Ngo, M. N. Dao, X. Dang, C. Wang, and M. Matthaiou, "Joint user association and power control for cell-free massive MIMO," *IEEE Internet of Things Journal*, vol. 11, no. 9, pp. 15 823–15 841, 2024.
- [11] M. S. A. Khan, S. Agnihotri, and R. Karthik, "Joint AP-UE association and power factor optimization for distributed massive MIMO," in *Proc. IEEE PIMRC*, Valencia, Spain, Sept. 2024.
- [12] J. Zhang, J. Zhang, E. Björnson, and B. Ai, "Local partial zero-forcing combining for cell-free massive MIMO systems," *IEEE Trans. on Commun.*, vol. 69, no. 12, pp. 8459–8473, 2021.
- [13] S. Chen, J. Zhang, E. Björnson, Ö. T. Demir, and B. Ai, "Sparse large-scale fading decoding in cell-free massive MIMO systems," in *Proc. IEEE SPAWC*, Oulu, Finland, July 2022.
- [14] M. Razaviyayn, "Successive convex approximation: Analysis and applications," Ph.D. dissertation, University of Minnesota, 2014.
- [15] K. Shen and W. Yu, "Fractional programming for communication systems—part II: Uplink scheduling via matching," *IEEE Trans. on Signal Processing*, vol. 66, no. 10, pp. 2631–2644, 2018.